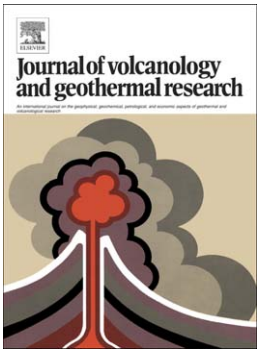

Discriminating the-long distance dispersal of fine ash from sustained columns or near ground ash clouds: the example of the Pomici di Avellino eruption (Somma-Vesuvius, Italy)

Roberto Sulpizio, Rosanna Bonasia, Pierfrancesco Dellino, Mauro A. Di Vito, Luigi La Volpe, Daniela Mele, Giovanni Zanchetta, Laura Sadori

PII: S0377-0273(07)00362-9
DOI: doi: 10.1016/j.jvolgeores.2007.11.012
Reference: VOLGEO 3795

To appear in: *Journal of Volcanology and Geothermal Research*

Received date: 5 March 2007
Revised date: 24 October 2007
Accepted date: 2 November 2007

Please cite this article as: Sulpizio, Roberto, Bonasia, Rosanna, Dellino, Pierfrancesco, Di Vito, Mauro A., La Volpe, Luigi, Mele, Daniela, Zanchetta, Giovanni, Sadori, Laura, Discriminating the-long distance dispersal of fine ash from sustained columns or near ground ash clouds: the example of the Pomici di Avellino eruption (Somma-Vesuvius, Italy), *Journal of Volcanology and Geothermal Research* (2007), doi: 10.1016/j.jvolgeores.2007.11.012

Discriminating the-long distance dispersal of fine ash from sustained columns or near ground ash clouds: the example of the Pomici di Avellino eruption (Somma-Vesuvius, Italy).

Roberto Sulpizio[1], Rosanna Bonasia[1], Pierfrancesco Dellino[1], Mauro A. Di Vito[2], Luigi La Volpe[1], Daniela Mele[1], Giovanni Zanchetta[3], Laura Sadori[4]

[1] CIRISIVU, c/o Dipartimento Geomineralogico,, via Orabona 4, 70125, Bari, Italy

[2] Istituto Nazionale di Geofisica e Vulcanologia, via Diocleziano 3284, Napoli, Italy

[3] Dipartimento di Scienze della Terra, via S. Maria 53, 56126, Pisa, Italy

[4] Dipartimento di Biologia Vegetale, Università La Sapienza, Piazza A. Moro 5, 00185, Roma, Italy

Abstract

Ash samples from tephra layers correlated with the Pomici di Avellino (Avellino Pumice) eruption of Somma-Vesuvius were collected in distal archives and their composition and particle morphology investigated in order to infer their behaviour of transportation and deposition. Differences in composition and particle morphologies were recognised for ash particles belonging to the magmatic Plinian and final phreatomagmatic phases of the eruption. The ash particles were dispersed in opposite directions during the two different phases of the eruption, and these directions are also different from that of coarse-grained fallout deposits. In particular, ash generated during magmatic phase and injected in the atmosphere to form a sustained column shows a prevailing SE dispersion, while ash particles generated during the final phreatomagmatic phase and carried by pyroclastic density currents show a general NW dispersion. These opposite dispersions indicate an ash dispersal influenced by both high and low atmosphere dynamics. In particular, the magmatic ash dispersal was first driven by stratospheric wind towards NE and then the falling particles

encountered a variable wind field during their settling, which produced the observed preferential SE dispersal. The wind field encountered by the rising ash clouds that accompanied the pyroclastic density currents of the final phreatomagmatic phase was different with respect to that encountered by the magmatic ash, and produced a NW dispersal. These data demonstrate how ash transportation and deposition are greatly influenced by both high and low atmosphere dynamics. In particular, fine-grained particles transported in ash clouds of small-scale pyroclastic density currents may be dispersed over distances and cover areas comparable with those injected into the stratosphere by Plinian, sustained columns. This is a point not completely addressed by present day mitigation plans in case of renewal of activity at Somma-Vesuvius, and can yield important information also for other volcanoes potentially characterised by explosive activity.

Keywords: Pomici di Avellino eruption, ash dispersal, atmosphere dynamics, volcanic hazard, tephra layers

1. Introduction

Volcanic ash (diameter < 2 mm) is the result of intense magmatic or phreatomagmatic fragmentation during explosive eruptions. After injection into the atmosphere, the ash is dispersed as convective columns and umbrella clouds, which are subjected to the combined effects of gravity and wind speed, or are transported close to the ground as pyroclastic density currents (e.g. Cas and Wright, 1987). Irrespective of the eruptive mechanism or intensity, ash particles usually affect wide areas around volcanic centres, and have a greater mobility than the coarse-grained parental deposits. This is mainly due to the effect of atmospheric viscosity that influences their settling behaviour in much more efficient way than that of coarse-grained and heavier particles (Bonadonna et al., 1998;

Dellino et al., 2005). Furthermore, the longer time of residence in the atmosphere with respect to the coarse particles allows also low-altitude, highly variable winds to have an important role in the dispersal behaviour of fine ash.

Research in genesis, dispersal and accumulation of ash during and after explosive eruptions is topic in the current research in volcanology (e.g. Zimanowski et al., 2001). Fine ash preserve important information about fragmentation mechanisms and energy budget of the eruption (Dellino and La Volpe, 1995; Buttner et al., 2006). Dispersal and deposition of ash has also serious implications when dealing with volcanic hazard evaluation. The accumulation of ash can induce roof collapses (e.g. Blong, 2003), interruption of lifelines (roads, railways, etc.), closure of airports and noise to communication or electric lines (e.g. Blong, 1984). The injection of ash into the atmosphere can cause damage to aircraft or can impact public health causing, for example, respiratory problems (e.g. Horwell et al., 2003; Horwell and Baxter, 2006). Ash deposition decreases soil permeability, increases surface runoff, and promotes floods (Zanchetta et al., 2004; Favalli et al., 2006). Ash leachates (Dahlgren et al., 1999; Armienta et al., 2002; Witham et al., 2005) can result in pollution of water resources (Stewart et al., 2006), damage to agriculture and forest, impact pasture and livestock health, impinge on aquatic ecosystems and alter the geochemical environment of the seafloor (e.g. Haekel et al., 2001). All these processes and impacts call for a care consideration in assessing volcanic hazard over large areas far beyond the volcano surroundings.

Despite some recent advances in understanding the impact of fine ash on environment and infrastructure (e.g. Blong, 1984; Haekel et al., 2001; Witham et al., 2005; Stewart et al., 2006), the dynamic of dispersal of fine ash remains poorly understood, and consideration of the associated hazards have not yet been fully addressed and included in the mitigation plans.

The Pomici di Avellino (PdA) eruption of Somma-Vesuvius (Lirer et al., 1973; Santacroce, 1987; Cioni et al., 2000) represents an unique opportunity to shed light on dispersal of fine ash during explosive eruptions. This is because the PdA eruption was characterised by two clearly distinct eruptive phases: an initial sustained column phase driven by magmatic fragmentation and

dominated by fall deposits, and a final phreatomagmatic phase dominated by generation of pyroclastic density currents (Cioni et al., 2000). Furthermore, ash particles generated during the two phases have different, idiosyncratic morphologies and partially different chemical composition, which make their detection and discrimination of the respective eruptive phase straightforward even in distal archives.

This paper deals with the morphologic and compositional study of distal ash (tephra layers) of PdA eruption recognised in different archives from central and southern Italy (Fig. 1). Morphology and composition of these distal tephra layers demonstrate how small-volume PDCs can disperse fine ash at distances comparable with those commonly reached by particles dispersed by high-altitude sustained columns.

2. Outline of Pomici di Avellino eruption

2.1. Proximal stratigraphy

The PdA eruption of Somma-Vesuvius (Lirer et al., 1973; Santacroce, 1987; Cioni et al., 2000) occurred during the Ancient Bronze Age (Cioni et al., 2000), and has a best estimated maximum age of 3930 ± 20 ^{14}C yr BP (4370 ± 40 cal yr BP; Santacroce et al., this volume). Cioni et al. (2000) divided the stratigraphic succession in three main phases (opening, magmatic Plinian and phreatomagmatic; Fig. 2), and five Eruption Units (EU1 to 5; Fig. 2; *sensu* Fisher and Schminke, 1984), which represent the most recent and complete description of the PdA eruption. Based on a more detailed stratigraphy of the final phreatomagmatic succession, four main depositional units can be identified within EU5 (from a to d; Fig. 2). In particular, the interbedding of fine ash at different heights within the EU5 succession helped in the identification of the different depositional units.

Fallout deposits dominate the opening and magmatic Plinian phases, while PDC deposits represent the most part of the last erupted deposits (phreatomagmatic phase). A pair of white pumice lapilli and brownish ash deposits occur at the very base of the stratigraphic succession, defining the opening phase of the eruption (EU1a and b; Fig. 2). Their dispersal is limited to few km in NE direction. The main fallout deposits, emplaced during the magmatic Plinian phase, comprise well-sorted pumice lapilli with abundant accidental lithics, which show a sharp change in colour from white at the base (EU2; Fig. 2) to grey at the top (EU3; Fig. 2). Both fans of fallout deposits have a NE direction, and dispersed coarse ash and lapilli over a narrow area across the southern Italy (Fig. 1). Assessed peak mass discharge rate was of $5.7x10^7$ kg/s during EU2 and $1.7x10^8$ kg/s during EU3, which correspond to column heights of 23 and 31 km respectively (Cioni et al., 2000).

Only one, small PDC interbeds the Plinian succession, and crops out at about half height of the EU3 deposits (Fig. 2). A thin, fallout deposit of pumice and lithic lapilli (EU4; Fig. 2), occurs at the top of the EU3 deposits, and closes the magmatic Plinian phase of the eruption (Fig. 2). It dispersed few centimetres of coarse ash and lapilli up to a distance of around 15 km in NE direction (Cioni et al., 2000). PDC deposits dominate the phreatomagmatic part of the stratigraphic succession. They are mainly fine-grained, massive to dune-bedded ash deposits with internal cross-stratification, which show a prevalent western and north-western dispersion (Fig. 1). Ten centimetres of coarse and fine ash have been recognised up to a distance of more than 20 km from the volcano slopes.

2.2. Distal tephra layers of the Avellino eruption

In the last decade, distal tephra layers related to the Avellino eruption have been recognised in both marine and lacustrine archives (Calanchi et al., 1996; 1998; this volume; Ramrath et al., 1999; Wulf et al., 2004; Drescher-Schneider et al., 2006; Lowe et al., 2007; Magny et al., 2007). Among these tephra layers, only TM4 from Lago Grande di Monticchio succession (Wulf et al., 2004) preserves an internal lithology similar to the proximal deposits, which comprises white pumice at the base (EU2) and grey ash at the top (EU3). Other lacustrine tephra layers occur as thin fine-ash layers,

usually light-brown or light-grey in colour, which mainly comprise glass shards and blocky glass fragments (Calanchi et al., 1996; Ramrath et al., 1999; Drescher-Schneider et al., 2006; Magny et al., 2007). Their very limited thickness usually prevented any accurate lithological description, and then a precise correlation with proximal EUs, which can only be inferred by composition of glass shards. The same difficult in correlating distal deposits with a certain EU still holds also for marine tephra layers recognised in cores from the Adriatic sea, in which they usually occur as cryptotephra dispersed in the sediments (Calanchi et al., 1998; this volume; Lowe et al., 2007). Therefore, the correlation of these marine and lacustrine tephra layers is often inferred by combining and assessing the consistency of compositional, lithological and chronological data (Table 1). It is important to note that the assignment of tephra layer from Adriatic sea core IN68-30 (20 cm depth; Table 1) has here been reinterpreted, because it was previously correlated to one of the AP eruptions (Calanchi et al., 1998; this volume). The new attribution is based on compositional matching with EU3 deposits of PdA eruption and on the absence of leucite crystals in the groundmass of the 20 cm depth tephra layer, which is characteristic of AP related tephras (Andronico and Cioni, 2003).

3. Analytical methods

Samples of distal tephra layers of PdA deposits were collected at Pian di Pecore, Basento and Lago di Mezzano sites (Fig. 1). Grain size distribution of deposits from Basento and Pian di Pecore sites were obtained using a Coulter multisizer (Beckman Coulter Inc., USA) in the fractions between 2.0 and 6.5 ϕ (250 – 11.2 μm). Grain size parameters were calculated using the program GRADISTAT (Blott and Pye, 2001).

Energy-dispersive-spectrometry (EDS) analyses of glass shards and glasses from pumice fragments were performed at the Dipartimento di Scienze della Terra (University of Pisa), using an EDAX-DX micro-analyser mounted on a Philips SEM 515 (operating conditions: 20 kV acceleration

voltage, 100s live time counting, 10^{-9} A beam current, beam diameter ~ 500 μm, 2100 shots per second, ZAF correction). The ZAF correction procedure does not include natural or synthetic standards for reference, and requires the analyses normalization at a given value (which is chosen at 100%). Analytical precision is of 0.5 % for abundances higher than 15 wt. %, 1 % for abundances around 5 wt. %, 5 % for abundances of 1 wt. %, and less than 20 % for abundances close to the detection limit (around 0.5 wt. %). Accuracy of measurements is around 1 %, a value analogue to that obtained using wave dispersion spectroscopy (WDS), as tested by Marianelli and Sbrana (1998). Comparison of EDS and WDS micro-analyses carried out on the same samples has shown differences less than 1 % for abundances greater than 0.5 wt. %.

Morphology of ash fragments was examined by scanning electron microscopy (SEM), to try to discriminate between magmatic and phreatomagmatic fragmentation (Buttner et al., 1999), and to yield information about the post-fragmentation history of juvenile fragments (Dellino and La Volpe 1995). Particularly suitable for morphology investigations are ash particles between ϕ 3.5 (0.090 mm) and ϕ 3 (0.125 mm; Dellino and La Volpe 1995), but fragments less than 50 μm were examined for samples from Pian di Pecore, Basento and Lago di Mezzano sites due to the fine grain size of distal tephra deposits.

4. Results

The correlation of distal tephra layers with PdA deposits has been established, basing on stratigraphic position and chronology (Table 1), coupled with chemical composition of glass (Tables 2, 3 and 4) and mineral phases. Inspection of EDS chemical analyses listed in Tables 2-4 show that composition of glass from proximal fallout deposits (white and grey pumice deposits, Fig. 2) have a peculiar high content in Al_2O_3 (mainly in the range 21-24%, Table 2) associated with a main range in SiO_2 content of 55-57 %, while the mean content of Fe_{tot} doubles its abundance

from white pumice (1.5 %) to grey ones (3 %) and CaO triplicates (1.6-5.5 %; Table 2). Samples from final phreatomagmatic phase (EU5, Fig. 2) show a double composition, with part of the analyses that matches the composition of glass from EU2 and EU3 deposits (EU5α; Table 2), and part that has a more evolved composition, reaching 68 % in SiO_2 (EU5β, Table 2). The peculiar composition of EU5 deposits is particularly evident in silica versus alkali ratio and CaO (Fig. 3a, b), and Al_2O_3 versus CaO and Fe_{tot} diagrams (Fig. 3c, d). The composition of EU5-β samples plot outside the compositional liquid lines that can be traced between the EU2 and EU3 products (Fig. 3b, c, and d). Indeed, in the Al_2O_3 versus CaO and Fe_{tot} diagrams (Fig. 3c, d) the EU5-β samples seem to describe a different evolutionary trend with respect t the other samples of PdA eruption. If we consider the glass composition of the other Somma-Vesuvius eruptions Santacroce et al. (this volume), the EU5-β samples match only that of the Schiava eruption, a poorly known explosive event recently attributed to the ancient Somma-Vesuvius activity (about 36 cal. ka BP; Di Vito et al., this volume; Santacroce et al., this volume). Thick (around 60 m) ashy deposits of Schiava eruption were drilled in the Camaldoli della Torre area (Di Renzo et al., 2007), located very close to the southern rim of the Piano delle Ginestre area (the vent area of PdA; Cioni et al., 2000; Fig. 1). The high explosivity that characterised the final phreatomagmatic phase of PdA eruption (Cioni et al., 2000) could have facilitated the mechanical crushing of the weak ashy deposits of the Schiava eruption, which were then entrapped in the eruptive mixture in the same way as the other lithic fragments of the volcanic and bedrock pile. Glass shards of Schiava eruption are usually crystal free, Y-shaped or curved fragments quite similar to those of the EU2 deposits of PdA eruption, and their visual distinction under the optical or electronic microscope is impossible. Therefore, the evolved glass composition of EU5-β can be considered as due to lithic components and not to be representative of the most evolved magma involved in the Avellino eruption. In any case, the EU5-β glass composition is a marker of the final phreatomagmatic phase of PdA eruption, since glass

shards with this evolved composition are absent in the samples from the magmatic phase of the eruption.

When plotted in the diagrams of Figure 3, the composition of the newly sampled deposits from Basento and Pian di Pecore sites overlaps that of proximal fallout deposits (Fig. 3, Table 3), whereas the glass from Lago di Mezzano site show a double composition similar to the EU5 deposits (Fig. 3; Table 3). Average analyses of already published data are less indicative of composition spectra, but they all plot in the magmatic fallout part of the diagrams (Fig. 3; Table 4).

Grain size analyses performed on sample from Pian di Pecore shows a polymodal, poorly sorted distribution, with a main mode at ϕ 2 (250 μm) and half of the material almost homogeneously distributed between ϕ 3 and ϕ 6.5 (125-11 μm; Fig. 4c). In turn, the sample from Basento basin site shows unimodal, well sorted frequency distributions, with modal value at ϕ 4.5 (Fig. 4d).

The morphoscopic analysis on samples from proximal deposits (EU2-3 and EU5), Lago di Mezzano, Pian di Pecore and Basento sites (Fig. 1) shows peculiar differences among the analysed fragments. Fragments from proximal fallout deposits are highly vesicular with fresh glass (neither adhering particles nor patinae are visible; Fig. 5a, b). In turn, fragments from EU5 proximal deposits are generally blocky, poorly vesicular, with cracks and adhering particles (Fig. 5c-f). Morphoscopic characteristics similar to those observed in proximal deposits can also be observed in fragments from distal tephra layers. In particular, the fragments from Basento and Pian di Pecore tephra layers are highly vesicular and with sharp and angular borders (Fig. 6a-d), while fragments from Lago di Mezzano tephra layer are blocky to poorly vesicular, and show chemical pitting on the clast surfaces (Fig. 6e-h).

5. Discussion

When dealing with correlation of distal tephra layers, one of the main source of error is the erroneous attribution of the tephra layers to proximal pyroclasts exhibiting similar composition and lithology but emplaced by different (even close in time) explosive eruptions (e.g. Siani et al., 2004). In the case of PdA tephra, the occurrence of at least three other widely dispersed tephra layers from Somma-Vesuvius slightly younger than PdA and with similar tephri-phonolitic composition (Proto-historic 1-3 or AP1-3 eruptions; Rolandi et al., 1998; Andronico and Cioni, 2002), enhances the probability of erroneous correlations. Some tephra layers related to APs eruptions were recognised in distal lacustrine (Wulf et al., 2004; Drescher-Schneider et al., 2006) and continental successions (Fig. 4a), and have lithology and composition similar to the PdA deposits. However, detailed inspection of glass composition of PdA and APs deposits shows how they can be discriminated using major elements chemistry, since AP products contain slight less SiO_2 and Al_2O_3, accompanied by an increase in Fe_{tot} with respect to the PdA ones (Fig. 7). An overlap of the two compositions exists in the range 55-56% of SiO_2 versus 3-4.5% of Fe_{tot} (75-78% SiO_2 plus Al_2O_3; Fig. 7), but it concerns the more evolved part of AP1 and AP2 deposits and the less evolved part of PdA deposits. Since these deposits are lithologically different (white pumice lapilli for AP1-2 deposits vs. grey-brown pumice lapilli for PdA deposits), simple field and laboratory observations of analysed material can help in confidently discriminate between the two possibilities. The analysis of mineral phases can add further elements for discriminating between PdA and AP tephra layers, because the first contains scapolite crystals (Cioni et al., 2000) that are absent in the second (Andronico and Cioni, 2002). Scapolite crystals were recognised in micropumice fragments sampled at Pian di Pecore site, confirming their correlation with the PdA deposits.

Once established the compositional-, mineralogical- and chronological-based correlation of the analysed tephra layers with the PdA deposits, the morphoscopic analysis of samples from Lago di Mezzano, Pian di Pecore and Basento sites (Fig. 1) allowed a precise attribution of the different tephra layers with either the magmatic Plinian or the final phreatomagmatic phase of the eruption. This is because fragments from the northward and southward dispersed tephra layers have different

diagnostic morphoscopic characteristics (Fig. 6). In particular, the particles from Pian di Pecore and Basento sites have morphologies, vesicularity and composition that indicate they were generated during the magmatic phase of the eruption. Since data from Lago Grande di Monticchio (TM-4 layer, Wulf et al., 2004) and from Adriatic sea (Calanchi et al., 1998) show homogeneous composition, which matches that of the magmatic phase of the eruption, follows that ash from this phase were dispersed towards south east (blue-shaded area in Fig. 8). On the other hand, compositional and morphological evidences (Table 3; Fig. 6) indicate that tephra layers recognised in lakes north of Somma-Vesuvius were dispersed during the final phreatomagmatic phase of the eruption (red-shaded area in Fig. 8).

These opposite directions of dispersal substantially diverge from those of coarse grained fallout deposits of EU2 and EU3, which show dispersions towards N65° and N55° respectively (Cioni et al., 2000; Fig. 8).

These evidences oblige to consider conditions of transport influenced by changing wind direction during the time-window between the end of the magmatic phase and the onset of the phreatomagmatic one. Furthermore, the distribution of magmatic ash (Fig. 8) indicates the influence of both high and low level winds (below 30 km of height) on their dispersal.

The settling of ash from a powerful, high Plinian column results in wider covered areas and in longer time of deposition with respect to the coarse grained particles (e.g. Walker 1973; Carey and Sparks, 1986; Pyle, 1989; Bonadonna and Phillips, 2003; Sulpizio, 2005). This longer settling time allows the prolonged and effective interaction of falling particles with low level winds, which can result in decoupling of falling coarse and fine particles, with preferential downwind deposition of the fine grained pyroclastics. This process can produce differences in content of fine particles in fallout deposits located upwind or downwind (e.g. Waitt et al, 1981; Sulpizio et al., 2005) and/or distortion of isopachs (e.g. Sulpizio et al., 2005). The grain size of particles effectively influenced by this process varies in function of aerodynamics characteristics of particles (Dellino et al., 2005), air viscosity (Bonadonna et al., 1998) and low-level wind speed. The inspection of grain size

distribution of a sample from EU3 fallout deposits collected 70 km downwind from the Somma-Vesuvius shows how it represents the coarser counterpart of the Basento sample, which is located around 160 km in SE direction (Fig. 8b). This is a compelling evidence, together with dispersal area of tephra layers from the magmatic phase of the eruption, which deposition of ash involved in the sustained column dynamic was influenced by low level wind that blew from NW to SE (blue arrow in Fig. 8). Further support to the hypothesis of variable wind field patterns with height is provided by the seasonal wind directions and speeds for southern Italy (Costa et al., 2007), which shows how low level winds are more variable in direction than stratospheric jets (Fig. 9). In particular, stratospheric jets statistically blow from west to east for the majority of the year, in agreement with the dispersal of coarse grained fallout deposits of PdA eruption (Fig. 8) and other large explosive eruptions of Somma-Vesuvius (Cioni et al., 2003). Beyond statistics, daily life experience demonstrates how low level winds can have very variable directions and speed, following local weather conditions, and this can alter significantly the distribution on land of fine grained deposits. Since powerful sustained columns did not occurred during the final phreatomagmatic phase (EU5), which was dominated by pyroclastic density current generation (Cioni et al., 2000), the dynamics of dispersal of fine ash was controlled by flow behaviour and atmospheric conditions that probably not included stratospheric jets. This is because the ability of a convective mixture to rise through the atmosphere is mainly function of balance between buoyancy-generated turbulence and gravitational force, and can be expressed by the mass flux (that carries both heat and mass) that fed the lofting plume (Wilson et al., 1980; Carey and Sparks, 1986; Wilson and Walker, 1987), which, for small size PDCs, is significantly lesser than that of the Plinian column. Weak volcanic plumes usually reach few km of height (e.g. Bonadonna et al., 2005; Scollo et al., 2007) and cannot cross the inversion layer that defines the top of the troposphere also in extra-tropical regions (e.g. Birner et al., 2002; Birner, 2006; Son and Polvani, 2007), which prevents the plume from rising higher. Similarly to the magmatic ash, also during the final phreatomagmatic phase the capability of fine ash to be maintained in suspension during transport in the atmosphere over long distances mainly

depends on maximum height reached in the atmosphere, intensity of driving wind and their aerodynamic properties. In the case of tephra layers related to EU5 PDCs, their dispersal indicates a wind direction towards NW (red arrow in Fig. 8).

6. Conclusions

The collected data on dispersal of ash from sustained columns and phoenix clouds of pyroclastic density currents demonstrated how the transport/deposition of fine grained material is a complex process, which includes aerodynamic characteristics of particles and dynamic of high and low atmosphere. This has great relevance when dealing with assessment of volcanic hazard, because these data demonstrate how wide distal areas, far beyond those affected by deposition of coarse-grained fallout and pyroclastic flow deposits, can be threatened by ash sedimentation. In particular, collected data demonstrate how centimetric ash blankets from phoenix plumes of small volume pyroclastic density currents can be dispersed hundred of kilometres away from the source area, a characteristic to date described only for large ignimbrite eruptions. Since ash deposition is a major problem in case of explosive eruptions (e.g. Blong, 1984; Haekel et al., 2001; Horwell and Baxter, 2006), and hazard evaluation plans at Somma-Vesuvius is based on dispersal of coarse-grained fallout deposits (e.g. Cioni et al., 2003) and proximal pyroclastic flow deposition (Santacroce et al., 1998), future mitigation plans must include additional hazards related to dispersion of ash driven by high and low atmosphere dynamics.

Acknowledgements

This work is part of the ongoing research on explosive volcanic activity of Italian volcanoes funded by Dipartimento della Protezione Civile and Istituto Nazionale di Geofisica e Vulcanologia of Italy

(DPC-INGV sub-project V3-4). Daniela Pantosti is acknowledged for helpful discussions and for providing samples of the Pian di Pecore site. David Pyle, Gianluca Sottili and an anonymous reviewer are acknowledged fro the useful review of the manuscript

References

Andronico, D., Cioni, R., 2002. Contrasting styles of Mount Vesuvius activity in the period between the Avellino and Pompeii Plinian eruptions, and some implications for assessment of future hazards. Bull. Volcanol. 64, 372–391 DOI 10.1007/s00445-002-0215-4

Armienta, M.A., De la Cruz-Reyna, S., Morton, O., Cruz, O., Ceniceros, N.; 2002. Chemical variations of tephra-fall deposit leachates for three eruptions from Popocatepetl volcano. J. Volcanol. Geotherm. Res. 113, 61-80.

Birner, T., A. Dörnbrack, and U. Schumann, 2002: How sharp is the tropopause at midlatitudes?, Geophys. Res. Lett., 29(14), 1700, doi:10.1029/2002GL015142.

Birner, T., 2006: Fine-scale structure of the extratropical tropopause region, J. Geophys. Res., 111, D04104, doi:10.1029/2005JD006301.

Blong, R.J., 1984. Volcanic hazards. A Sourcebook on the Effects of Eruptions. Academic Press, Sydney. 424 pp.

Blong, R., 2003. Building damage in Rabaul, Papua New Guinea, 1994. Bull. Volcanol. 65, 43–54.

Blott, S.J. and Pye, K., 2001. GRADISTAT: a grain size distribution and statistic package for the analysis of unconsolidated sediments. Earth Surf. Process. Landforms, 26, 1237-1248.

Bonadonna, C., Ernst, G.G.J., Sparks, R.S.J., 1998. Thickness variation and volume estimates of tephra fall deposits: the importance of particle Reynolds number. J. Volcanol. Geotherm. Res. 81, 173-187.

Bonadonna, C., Phillips, J.C., 2003. Sedimentation from strong volcanic plumes. J. Geophys. Res. 108, B7, 2340, doi:10.1029/2002JB002034,

Bonadonna, C., Phillips, J.C., Houghton, B.F., 2005. Modelling tephra sedimentation from a Ruapehu weak plume eruption. J. Geophys. Res. 110, B08209, doi:10.1029/2004JB003515.

Buttner, R., Dellino, P., Zimanowski, B., 1999. Identifying modes of magma/water interaction from the surface features of ash particles. Nature, 401, 688– 690.

Buttner, R., Dellino, P., Raue, H., Sonder, I., Zimanowski, B., 2006. Stress-induced brittle fragmentation of magmatic melts: Theory and experiments. J. Geophys. Res., 111, B08204, doi:10.1029/2005JB003958,

Calanchi, N., Dinelli, E., Lucchini, F., Mordenti, A., 1996. Chemostratigraphy of the Late Quaternary sediments from Lake Albano and Central Adriatic Sea cores (PALICLAS project). Mem. Ist. Ital. Idrobiol. 55, 247-263.

Calanchi, N., Cattaneo, A., Dinelli, E., Gasparotto, G., Lucchini, F., 1998. Tephra layers in Late Quaternary sediments of the central Adriatic Sea. Marine Geology 149, 191–209.

Calanchi, N., Dinelli, E., 2007. Tephrostratigraphy for the last 170 ka in sedimentary successions from the Adriatic sea. J. Volcanol. Geotherm. Res., this volume.

Carey, S., Sparks, R.S.J., 1986. Quantitative models of the fallout and dispersal of tephra from volcanic eruption columns. Bull. Volcanol. 48, 109-125.

Cas, R., Wright, J.W., 1987. Volcanic Successions: Modern and Ancient. Allen and Unwin, London, 528 pp.

Chondrogianni C., Ariztegui, D., Bernasconi, S.M., Lafargue, E., McKenzie, J.A., 1996. Geochemical indicators tracing ecosystem response to climate change during the late Pleistocene (Lake Albano, central Italy). Mem. Ist ital. Idrobiol. 55, 99-110.

Cioni, R., Levi, S., Sulpizio, R., 2000. Apulian Bronze Age pottery as a long-distance indicator of the Avellino Pumice eruption (Vesuvius, Italy). In: Mc Guire W.G., Griffiths D.R., Hancock P.L., Stewart I.S. (eds) The Archaeology of Geological chatastrophes. Geological Society, London, Special Publications, 171, 159-177

Cioni, R., Longo, A., Macedonio, G., Santacroce, R., Sbrana, A., Sulpizio, R., Andronico, D., 2003. Assessing pyroclastic fall hazard through field data and numerical simulations: the example from Vesuvius. J. Gephys. Res. 108, doi:10.1029/2001JB000642.

Costa, A., Dell'Erba, F., Di Vito, M., Isaia, R., Macedonio, G., Orsi, G., Pfeiffer, T., 2007. Tephra fallout hazard assessment at the Campi Flegrei caldera (Italy). Bull. Volc., under revision.

Dade, B.W., Huppert, H.E., 1996. Emplacement of the Taupo Ignimbrite by a dilute turbulent flow. Nature. 381, 509–512.

Dahlgren, R. A., Ugolini, F.C., Casey, W. H., 1999. Field weathering rates of Mt. St. Helens tephra. Geoch. Cosmoch. Acta. 63, 587–598.

Dellino, P., La Volpe, L., 1995. Fragmentation versus transportation mechanisms in the pyroclastic sequence of Monte Pilato Rocche Rosse (Lipari, Italy). J. Volcanol. Geotherm. Res., 64, 211–231.

Dellino, P., Mele, D., Bonaria, R., Braia, G., La Volpe, L., Sulpizio, R., 2005. The aerodynamics of pumice. Geophys. Res. Lett. 32, L21306, doi:10.1029/2005GL023954.

Di Renzo, V., Di Vito, M.A., Arienzo, I., Carandente, A., Civetta, L., D'Antonio, M., Giordano, F., Orsi, G., Tonarini, S., 2007. Magmatic history of Somma-Vesuvius on the basis of new geochemical and isotopic data from a deep borehole (Camaldoli della Torre). J. Petrol., 48, 753-784.

Di Vito, M.A., Sulpizio, R., Zanchetta, G., D'Orazio, M., 2007. The late Pleistocene pyroclastic deposits of the Campanian Plain: new insights into the explosive activity of Neapolitan volcanoes. J. Volcanol. Geotherm. Res., this volume.

Drescher-Schneider, R., De Beaulieu, J.L, Magny, M., Walter-Simonnet, A.V., Bossuet, G., Millet, L., Brugiapaglia, E., Drescher, A., 2006. Vegetation history, climate and human impact over the last 15 000 years at Lago dell'Accesa (Tuscany, Central Italy). Veget. Hist. Archaeobot. DOI 10.1007/s00334-006-0089-z

Favalli, M., Pareschi, M. T., Zanchetta, G., 2006. Simulation of syn-eruptive floods in the circumvesuvian plain (southern Italy). Bull. Volcanol., 68, 349–362.

Fisher, R.V., Schmincke, H.U., 1984. Pyroclastic rocks. Springer-Verlag, Berlin, 472 pp.

Haekel, M., van Beusekom, J., Wiesner, M.G., Konig, I., 2001. The impact of the 1991 Mount Pinatubo tephra fallout on the geochemical environment of the deep-sea sediments in the South China Sea. Earth Plan. Sc. Lett. 193, 151-166.

Horwell, C.J., Sparks, R.S.J., Brewer, T.S., Llewellin, E.W., Williamson B.J., 2003. Characterization of respirable volcanic ash from the Soufriére Hills volcano, Montserrat, with implications for human health hazards. Bull. Volcanol. 65: 346–362.

Horwell, C.J., Baxter, P.J., 2006. The respiratory health hazards of volcanic ash: a review for volcanic risk mitigation. Bull. Volcanol., 69, 1–24, DOI 10.1007/s00445-006-0052-y

Lirer, L., Pescatore, T., Booth, P., Walker, J.P.L., 1973. Two Plinian pumice fall deposits from Somma–Vesuvius, Italy. GSA Bulletin, 84, 759–772.

Langone, L.A., Asioli, A., Correggiari, A., Trincardi, F., 1996. Age-depth modelling through the late Quaternary deposits of the central Adriatic basin. Mem. Ist. Ital. Idrobiol. 55, 177-196.

Lowe, J.J., Blockley, S., Trincardi, F., Asioli, A., Cattaneo, A., Matthews, I.P., Pollard, M., Wulf, S., 2007. Age modelling of late Quaternary marine sequences in the Adriatic: towards improved precision and accuracy using volcanic event stratigraphy. Cont. Shelf Res., 27, 560–582.

Magny, M., de Beaulieu, J.L., Drescher-Schneider, R., Vanniére, B., Walter-Simonnet, A.V., Miras, Y., Millet, L., Bossuet, G., Peyron, O., Brugiapaglia, E., Leroux, A., 2007. Holocene climate changes in the central Mediterranean as recorded by lake-level fluctuations at Lake Accesa (Tuscany, Italy). Quat. Sc. Rev., 26, 1736–1758.

Marianelli, P., Sbrana, A., 1998. Risultati di misure di standard di minerali e di vetri naturali in microanalisi a dispersione di energia. Atti Soc. Tosc. Sc. Nat. Mem., Serie A, 105, 57-63.

Pantosti, D., Schwartz, D.P., Valenzise, G., 1993. Paleoseismology along the 1980 rupture of the Irpinia fault. J. Geophys. Res., B4 98, 6561-6577.

Pyle, D.M., 1989. The thickness, volume and grainsize of tephra fall deposits. Bull. Volcanol., 51, 1-15.

Ramrath, A., Zolitschka, B., Wulf, S., Negendank, J.F.W., 1999. Late Pleistocene climatic variations as recorded in two Italian maar lakes (Lago di Mezzano, Lago Grande di Monticchio). Quat. Sc. Rev., 18, 977-992.

Rolandi, G., Petrosino, P., McGeehin, J., 1998. The interplinian activity at Somma-Vesuvius in the last 3,500 years. J. Volcanol. Geotherm. Res., 82, 19–52.

Santacroce, R. (ed.), 1987. Somma-Vesuvius, Quaderni de la Ricerca Scientifica, CNR, 114, Progetto Finalizzato Geodinamica, Monografie Finali, 8.

Santacroce, R., Andronico, D., Cavarra, L., Cioni, R., Favalli, M., Longo, A., Macedonio, G., Pareschi, M.T., Sbrana, A, Sulpizio, R., Zanchetta, G., 1998. Updating the scenario of the mid-term maximum expected eruption of Vesuvius. Proceedings of Cities on Volcanoes International meeting. Rome and Naples, June 28- July 4, 1998, 119.

Santacroce, R., Cioni, R., Marianelli, P., Sbrana, A., Sulpizio, R., Zanchetta, G., Donahue, D.J., 2007. Chronology and composition of Vesuvius pyroclasts: a tool for distal tephrostratigraphy. J. Volcanol. Geoth. Res., this volume.

Scollo, S., Del Carlo, P., Coltelli, M., 2007. Tephra fallout of 2001 Etna flank eruption: analysis of the deposit and plume dispersion. J. Volcanol. Geotherm. Res., 160, 147–164.

Siani G., Sulpizio R., Paterne M., Sbrana, A., 2004. Tephrostratigraphy study for the last 18,000 ^{14}C years in a deep-sea sediment sequence for the South Adriatic. Quat. Sc. Rev. 23, 2485-2500.

Son, S.W., Polvani, L.M., 2007. Dynamical formation of an extra-tropical tropopause inversion layer in a relatively simple general circulation model. Geophys. Res. Lett., 34, L17806, doi: 10.1029/2007GL030564

Stewart, C., Johnston, D.M., Leonard, G.S., Horwell, C.J., Thordarson, T., Cronin, S.J., 2006. Contamination of water supplies by volcanic ashfall: a literature review and simple impact modelling. J. Volcanol. Geoth. Res., 158, 296-306.

Sulpizio, R., 2005. Three empirical methods for the calculation of distal volume of tephra-fall deposits. J. Volcanol. Geoth. Res. 145, 315-336.

Sulpizio, R., Mele, D., Dellino, P., La Volpe, L., 2005. A complex, Subplinian-type eruption from low-viscosity, phonolitic to tephri-phonolitic magma: the AD 472 (Pollena) eruption of Somma-Vesuvius (Italy). Bull. Volcanol. DOI 10-1007/s00445-005-0414-x.

Walker, G.P.L., 1973. Explosive volcanic eruptions—a new classification scheme. Geol. Rundsch. 62, 431–446.

Wilson, L., Sparks, R.S.J., Walker, G.P.L., 1980. Explosive volcanic eruptions-IV. The control of magma properties and conduit geometry on eruption column behaviour. Geophys. J. R. Astron. Soc., 63, 117-148.

Wilson, L., Walker, G.P.L., 1987. Explosive volcanic eruptions-IV. Ejecta dispersal in Plinian eruptions. The control of eruption conditions and atmospheric properties. Geophys. J. R. Astron. Soc., 89, 657-679.

Witham, C.S., Oppenheimer, C., Horwell, C.J., 2005. Volcanic ash-leachates: a review and recommendations for sampling methods. J. Volcanol. Geotherm. Res., 141, 299–326.

Wulf, S., Kraml, M., Brauer, A., Keller, J., Negendank, J.F.W., 2004. Tephrochronology of the 100 ka lacustrine sediment record of Lago Grande di Monticchio (southern Italy). Quat. Int., 122, 7–30.

Waitt, R.B., Hansen, V.L., Sarna-Wojcicki, A., Wood, S.H.,1981. Proximal air-fall deposits of eruptions between May 24 and August 7, 1980 – Stratigraphy and field sedimentology. U.S. Geol. Surv. Prof. Pap. 1250, 577-600.

Zanchetta, G., Sulpizio, R., Di Vito, M.A., 2004. The role of volcanic activity and climate in alluvial fan growth at volcanic areas: an example from southern Campania (Italy). Sedim. Geol. 168, 249-260.

Zimanowski, B., Wohletz, K., Dellino, P., Buttner, R., 2001. The volcanic ash problem. J. Volcanol. Geotherm. Res., 122, 1-5.

Figure captions

Figure 1 – Location map of the studied sites. The 1 cm isopachs of white and grey pumice fallout deposits are reported as white and black ellipses, respectively (from Cioni et al., 2000). In the framework in the upper right angle is reported a schematic dispersion of proximal pyroclastic density current deposits from the final phreatomagmatic phase (thickness in cm). The thick black line delimits the Piano dell Ginestre area. Grey circle indicates the inferred vent of PdA eruption. CdT= Camaldoli della Torre drilling point.

Figure 2 – Schematic stratigraphic succession of the Pomici di Pomici di Avellino eruption.

Figure 3 – SiO_2 vs. alkali ratio and CaO, and Al_2O_3 vs. CaO and Fe_{tot} diagrams for proximal and distal deposits of the Avellino eruption. The dashed lines in Al_2O_3 vs. Fe_{tot} diagram indicates liquid lines of descent. The letters α and β indicate two different compositions found in the phreatomagmatic deposits of the proximal area (EU5) and in the tephra layer from Lago di Mezzano. The label EU2+EU3 indicates the composition of proximal fallout deposits. Av=average data. RF93-30 from Calanchi et al., 1998; TM4 from Wulf et al., 2004; Nemi from CAlanchi et al., 1996; Schiava from Santacroce et al., this volume.

Figure 4 – Distal tephra layers and grain size data. a) Pomici di Avellino tephra layer at Basento basin site. Note the overlying tephra layer of AP3 eruption (2710 ± 60 ^{14}C yr BP; Rolandi et al., 1998) from Somma-Vesuvius. The scale is two meters long; b) Exposure of ash from Pomici di Avellino eruption at Pian di Pecore site; c) grain size distribution of ash collected at Pian di Pecore site; d) grain size distribution of ash collected at Basento basin site.

Figure 5 – Scanning electron microscope images of particles from proximal magmatic (a and b) and phreatomagmatic (c-f) deposits of Pomici di Avellino eruption.

Figure 6 - Scanning electron microscope images of particles from distal tephra layers; a-b) Basento site; c-d) Pian di Pecore site; e-h) Lago di Mezzano site.

Figure 7 – SiO_2 vs. Fe_{tot} and SiO_2+Al_2O_3 vs. Fe_{tot} diagrams of Pomici di Avellino and APs eruptions. TB1=Pomici di Avellino tephra from basento basin; TB2=AP3 tephra from Basento basin. AP data from Andronico and Cioni (2002), EU2 and EU3 proximal data from Santacroce et al. (this volume).

Figure 8 – Different dispersal areas of ash from magmatic Plinian (blue shaded area) and final phreatomagmatic (red shaded area) phases of the eruption. The 1 cm isopachs of white and grey pumice fallout deposits are reported as white and black ellipses, respectively (from Cioni et al., 2000). Arrows indicate the inferred direction of stratospheric and lower levels winds during the different phases of the eruption. White arrow=direction of stratospheric winds during EU2 deposition; Black arrow= direction of stratospheric winds during EU3 deposition; Blue arrow= direction of low level winds during EU3 deposition; Brown arrow=direction of low level winds during pyroclastic density current generation during the final phreatomagmatic phase. A sketch of wind azimuths during the different eruptive phases is shown in the lower left corner. Grain size distributions of EU3 fallout deposits sampled at ca 70 km from the vent and tephra layers from basento and Pian di Pecore sites are reported in the inserted diagrams. X axis indicates grain size expressed as ϕ units, while Y-axis indicates % of abundance.

Figure 9 – Seasonal and whole year atmospheric wind direction at 5, 10, 20, and 30 km of altitude recorded at xx meteorological station (from Costa et al., 2007, modified).

Table captions

Table 1 – Summary of the samples of distal tephra layers of Pomici di Avellino eruption used in this study.

Table 2 – EDS chemical analyses on glass of proximal samples of fallout (EU2 and EU3) and phreatomagmatic pyroclastic density current (EU5) deposits. The two different compositional groups found in EU5 deposits were distinguished with Greek letters α and β.

Table 3 - EDS chemical analyses on glass of distal tephra layers collected at Lago di Mezzano, Pian di Pecore and Basento basin sites. The two different compositional groups found in Lago di Mezzano sample were distinguished with Greek letters α and β.

Table 4 – Literature EDS and EPMA data of distal tephra layers of Pomici di Avellino eruption. RF93-30=sample from a central Adriatic marine core (Calanchi et al., 1998); IN68-9= sample from a south Adriatic marine core (Calanchi et al., this volume); LGM=lago Grande di Monticchio, tephra layer TM4 (EPMA data; Wulf et al., 2004); LNEMI=Lago di Nemi (Calanchi et al., 1996). Average EDS data of glass from proximal deposits of Pomici di Avellino eruption are reported for comparison.

Locality	sample	Inferred age (yr BP)	Calendar age (cal yr BP)[a]	Lithology	Thick.	Reference
Lago dell'Accesa	563 cm	Younger than 3910±30 Older than 3355±50	Younger than 4350±50 Older than 3590±70	Phonolitic glass shards with crystals of feldspar, biotite and pyroxene	not av.	Drescher-Schneider et al., 2006; Magny et al., 2007
Lago di Mezzano	-	3630±30	3950±40	Light brown ash layer, which comprises light coloured glass shards with vitric and/or microcrystalline groundmass and blocky fragments	1 cm	Ramrath et al., 1999; This work
Lago di Nemi	450 cm	4100 yr BP			3 cm	Chondrogianni et al., 1996; Calanchi et al., 1996
Marine core RF93-30	530 cm	Older than 3960±60 Younger than 5880±50	Older than 4410±100 Younger than 6280±50		not av.	Langone et al., 1996; Calanchi et al., 1998
Marine core IN68-30	20 cm	-			not av.	Calanchi et al., 1998; this volume
Lago Grande di Monticchio	TM-4	-	4310 (varve-based age)	Basal white pumice fallout deposits overlies by grey ash	0.6 cm	Wulf et al., 2004
Pian di Pecore	-	Younger than 3850±55 yr BP	Younger than 4280±100	Homogeneous light grey fine ash	30 cm	Pantosti et al., 1993; This work
Basento	TB1	-	-	Dark grey, loose, fine to coarse ash with sanidine, biotite and pyroxene crystals	3 cm	This work

EU2 (white pumice)

	SiO_2	TiO_2	Al_2O_3	FeO_{tot}	MnO	MgO	CaO	Na_2O	K_2O	ClO	Total	Tot. alkali	K_2O/Na_2O
1	53.92	0.46	23.57	1.08	0.29	0.00	1.66	10.08	7.10	1.20	99.36	17.18	0.70
2	55.14	0.10	24.07	1.05	0.13	0.00	1.20	11.09	6.62	0.55	99.95	17.71	0.60
3	55.76	0.00	24.20	1.20	0.00	0.00	1.17	9.93	6.95	0.67	99.88	16.88	0.70
4	56.22	0.00	22.87	2.01	0.21	0.00	1.98	6.00	9.84	0.81	99.94	15.84	1.64
5	55.66	0.17	23.76	1.81	0.17	0.00	1.73	5.69	10.09	0.88	99.96	15.78	1.77
6	55.59	0.00	23.64	2.11	0.25	0.00	2.10	4.55	10.63	1.01	99.88	15.18	2.34
7	56.28	0.00	23.83	1.83	0.00	0.00	1.83	5.25	9.87	0.95	99.84	15.12	1.88
8	56.04	0.00	23.97	1.36	0.00	0.00	1.47	8.10	8.10	0.81	99.85	16.20	1.00
9	56.78	0.00	23.77	1.94	0.25	0.00	1.91	4.56	9.66	0.98	99.85	14.22	2.12
10	54.57	0.19	22.16	2.53	0.25	0.00	2.25	5.66	11.31	1.03	99.95	16.97	2.00
11	58.42	0.00	24.47	1.69	0.00	0.00	1.58	4.30	8.42	0.94	99.82	12.72	1.96
12	57.27	0.22	24.10	1.98	0.26	0.00	2.05	3.73	9.26	1.08	99.95	12.99	2.48
13	56.75	0.13	24.24	0.86	0.00	0.00	1.17	9.51	6.63	0.62	99.91	16.14	0.70
14	59.53	0.00	24.68	1.53	0.00	0.00	1.61	3.86	7.67	0.98	99.86	11.53	1.99
15	56.14	0.00	24.27	1.33	0.17	0.00	1.38	7.98	7.80	0.83	99.90	15.78	0.98
16	59.49	0.00	24.49	1.40	0.00	0.00	1.50	4.20	8.02	0.91	100.01	12.22	1.91
17	60.05	0.13	24.84	1.74	0.17	0.00	1.83	2.72	7.54	0.95	99.97	10.26	2.77
18	60.23	0.00	25.00	1.44	0.21	0.00	1.48	3.54	7.12	0.92	99.94	10.66	2.01
19	56.55	0.11	23.16	1.39	0.12	0.00	1.74	7.28	8.90	0.70	99.95	16.18	1.22
20	57.64	0.18	23.10	1.26	0.00	0.00	1.66	6.45	8.98	0.66	99.93	15.43	1.39
21	57.94	0.17	22.82	1.68	0.18	0.00	2.12	3.98	10.27	0.79	99.95	14.25	2.58
22	57.48	0.00	23.41	1.90	0.17	0.00	1.90	3.44	10.76	0.76	99.82	14.20	3.13
23	55.96	0.00	23.93	1.33	0.21	0.00	1.47	8.19	7.95	0.82	99.86	16.14	0.97
24	56.22	0.15	24.24	1.05	0.00	0.00	1.32	8.99	7.22	0.71	99.90	16.21	0.80
25	57.54	0.14	23.52	1.30	0.00	0.00	1.44	7.59	7.48	0.81	99.82	15.07	0.99
26	56.05	0.00	24.29	1.18	0.16	0.00	1.34	7.79	7.43	0.74	98.98	15.22	0.95
27	56.03	0.00	23.90	1.25	0.12	0.00	1.35	8.66	7.78	0.77	99.86	16.44	0.90
28	58.83	0.13	24.19	1.28	0.00	0.00	1.51	5.95	7.19	0.85	99.93	13.14	1.21
29	55.87	0.10	24.34	1.44	0.11	0.00	0.99	9.47	7.41	0.25	99.98	16.88	0.78

EU3 (grey pumice)

	SiO_2	TiO_2	Al_2O_3	FeO_{tot}	MnO	MgO	CaO	Na_2O	K_2O	ClO	Total	Tot. alkali	K_2O/Na_2O
1	54.59	0.34	21.95	2.88	0.00	0.00	4.46	6.36	7.82	1.21	99.61	14.18	1.23
2	55.69	0.46	21.70	3.66	0.00	0.00	4.27	4.67	8.63	0.63	99.71	13.30	1.85
3	55.58	0.27	21.82	2.94	0.00	0.13	4.64	5.63	8.27	0.69	99.97	13.90	1.47
4	55.67	0.26	22.20	2.89	0.00	0.21	4.29	5.49	8.32	0.60	99.93	13.81	1.52
5	55.54	0.26	21.83	3.00	0.00	0.00	4.63	5.62	8.30	0.64	99.82	13.92	1.48
6	55.73	0.27	22.02	2.93	0.00	0.18	4.10	5.52	8.54	0.66	99.95	14.06	1.55
7	55.19	0.44	21.67	3.15	0.00	0.00	4.61	5.55	8.49	0.64	99.74	14.04	1.53
8	55.14	0.19	21.88	2.90	0.00	0.16	4.58	6.45	8.01	0.65	99.96	14.46	1.24
9	56.85	0.27	22.36	2.75	0.00	0.00	3.75	5.40	7.89	0.50	99.77	13.29	1.46
10	54.57	0.62	19.54	4.94	0.00	0.11	8.77	4.04	6.29	0.39	99.27	10.33	1.56
11	55.74	0.19	21.83	2.97	0.00	0.12	4.26	5.75	8.44	0.62	99.92	14.19	1.47
12	55.17	0.28	22.00	3.03	0.00	0.16	4.64	5.98	8.00	0.58	99.84	13.98	1.34
13	54.98	0.26	21.95	3.17	0.00	0.13	4.70	5.93	8.26	0.54	99.92	14.19	1.39
14	55.76	0.26	21.97	2.94	0.00	0.12	4.17	5.85	8.19	0.71	99.97	14.04	1.40
15	55.28	0.52	21.57	3.70	0.00	0.25	4.06	5.06	8.82	0.60	99.86	13.88	1.74
16	56.30	0.21	22.12	2.60	0.00	0.00	3.66	6.28	8.06	0.60	99.83	14.34	1.28
17	56.81	0.28	21.98	2.72	0.00	0.12	3.70	5.78	7.93	0.63	99.95	13.71	1.37
18	56.36	0.24	22.32	2.79	0.00	0.00	3.82	5.55	8.24	0.59	99.91	13.79	1.48
19	55.74	0.39	21.80	3.10	0.00	0.00	4.22	4.92	9.01	0.68	99.86	13.93	1.83
20	56.12	0.28	22.39	2.68	0.00	0.15	3.76	5.80	8.13	0.61	99.92	13.93	1.40

21	56.18	0.22	22.09	2.81	0.00	0.00	4.01	5.39	8.52	0.63	99.85	13.91	1.58
22	55.57	0.30	21.80	2.97	0.00	0.00	4.16	6.06	8.37	0.63	99.86	14.43	1.38
23	55.55	0.23	21.86	3.18	0.00	0.13	4.39	5.12	8.97	0.53	99.96	14.09	1.75
24	56.34	0.30	22.08	2.70	0.00	0.00	4.20	5.34	8.33	0.52	99.81	13.67	1.56
25	54.72	0.43	21.61	3.70	0.00	0.16	5.01	5.09	8.35	0.68	99.75	13.44	1.64
26	55.23	0.31	21.69	3.00	0.00	0.16	4.97	5.61	8.21	0.69	99.87	13.82	1.46
27	55.23	0.30	22.00	2.79	0.00	0.00	4.75	6.13	7.94	0.66	99.80	14.07	1.30
28	55.98	0.30	21.71	3.04	0.00	0.15	4.42	5.48	8.19	0.60	99.87	13.67	1.49

EU5a

	SiO_2	TiO_2	Al_2O_3	FeO_{tot}	MnO	MgO	CaO	Na_2O	K_2O	ClO	Total	Tot. alkali	K_2O/Na_2O
1	57.78	0.36	22.14	3.10	0.22	0.36	3.19	5.73	6.36	0.76	100.00	12.09	1.11
2	57.09	0.27	22.21	2.70	0.17	0.23	4.40	4.84	7.50	0.58	99.99	12.34	1.55
3	57.40	0.45	22.40	3.06	0.24	0.29	3.74	4.60	7.17	0.64	99.99	11.77	1.56
4	57.54	0.38	22.45	2.67	0.11	0.42	3.82	5.10	6.80	0.70	99.99	11.90	1.33
5	57.30	0.35	22.58	2.74	0.21	0.32	3.15	5.32	7.29	0.73	99.99	12.61	1.37
6	59.67	0.33	21.15	2.66	0.35	0.24	1.90	5.01	7.93	0.76	100.00	12.94	1.58
7	57.79	0.17	23.67	2.00	0.29	0.29	1.97	5.93	7.31	0.59	100.01	13.24	1.23
8	59.84	0.72	19.60	4.16	0.18	0.93	3.99	3.20	6.92	0.46	100.00	10.12	2.16
9	55.96	0.66	19.20	5.56	0.00	1.67	5.33	3.39	7.67	0.56	100.00	11.06	2.26
10	56.36	0.11	23.35	1.83	0.00	0.34	1.96	7.50	7.92	0.64	100.01	15.42	1.06
11	56.54	0.16	22.25	2.84	0.08	0.49	3.86	5.73	7.53	0.52	100.00	13.26	1.31
12	56.72	0.10	23.11	2.33	0.00	0.40	1.92	7.25	7.67	0.49	99.99	14.92	1.06
13	56.86	0.15	21.51	3.06	0.00	0.51	3.79	5.11	8.39	0.63	100.01	13.50	1.64
14	58.57	0.71	19.06	4.84	0.00	1.49	4.68	3.29	6.98	0.38	100.00	10.27	2.12
EU5b													
1	68.00	0.26	17.42	1.85	0.25	0.22	2.38	2.77	6.38	0.46	99.99	9.15	2.30
2	67.63	0.23	17.52	1.87	0.29	0.26	2.11	2.44	7.01	0.64	100.00	9.45	2.87
3	68.14	0.15	17.54	1.82	0.18	0.30	2.33	2.83	6.24	0.47	100.00	9.07	2.20
4	67.63	0.25	17.54	1.92	0.30	0.19	2.33	2.50	6.77	0.57	100.00	9.27	2.71
5	67.18	0.22	17.54	2.04	0.41	0.25	2.42	2.18	7.16	0.60	100.00	9.34	3.28
6	65.59	0.49	17.81	2.52	0.09	0.29	2.69	2.86	7.00	0.65	99.99	9.86	2.45
7	66.38	0.13	17.76	2.02	0.09	0.44	2.27	3.27	7.06	0.57	99.99	10.33	2.16
8	66.19	0.40	17.80	2.15	0.00	0.41	2.52	2.72	7.25	0.56	100.00	9.97	2.67
9	66.06	0.20	17.98	2.36	0.32	0.23	2.41	3.06	6.77	0.62	100.01	9.83	2.21
10	66.05	0.37	18.73	1.98	0.00	0.24	1.66	2.80	7.84	0.32	99.99	10.64	2.80
11	65.97	0.38	18.47	2.57	0.19	0.23	1.67	3.89	5.79	0.85	100.01	9.68	1.49
12	65.25	0.44	18.15	2.53	0.11	0.35	1.94	2.08	8.88	0.28	100.01	10.96	4.27
13	62.77	0.48	19.41	3.24	0.43	0.39	1.88	3.95	6.52	0.95	100.02	10.47	1.65
14	61.58	0.53	19.02	3.91	0.14	0.61	3.07	2.33	8.44	0.38	100.01	10.77	3.62
15	61.22	1.77	20.22	1.08	0.00	0.72	2.98	2.51	9.51	0.00	100.01	12.02	3.79

L. Mezzano a

	SiO_2	TiO_2	Al_2O_3	FeO_{tot}	MnO	MgO	CaO	Na_2O	K_2O	ClO	Total	Tot. alkali	K_2O/Na_2O
1	55.88	0.29	24.71	1.81	0.05	0.30	1.50	8.35	6.63	0.49	100.01	14.98	0.79
2	56.85	0.26	23.90	2.25	0.17	0.21	1.74	7.82	6.06	0.75	100.01	13.88	0.77
3	56.01	0.27	23.57	1.85	0.00	0.22	1.52	8.71	7.28	0.56	99.99	15.99	0.84
4	55.60	0.24	23.42	1.74	0.25	0.15	1.48	8.83	7.74	0.55	100.00	16.57	0.88
5	56.86	0.08	24.00	1.85	0.12	0.11	1.54	9.14	5.94	0.36	100.00	15.08	0.65
6	55.80	0.24	23.25	1.82	0.06	0.27	1.81	8.92	7.27	0.55	99.99	16.19	0.82
7	56.19	0.19	23.36	2.07	0.22	0.28	1.71	8.49	6.93	0.55	99.99	15.42	0.82
8	55.11	0.23	23.39	2.82	0.15	0.21	1.64	8.50	7.41	0.55	100.01	15.91	0.87
9	56.64	0.17	23.32	1.79	0.19	0.26	1.36	9.64	6.08	0.55	100.00	15.72	0.63
11	59.45	0.14	22.67	1.93	0.08	0.35	1.45	7.57	5.96	0.39	99.99	13.53	0.79
12	55.52	0.20	23.63	1.79	0.10	0.15	1.61	9.25	7.24	0.51	100.00	16.49	0.78
13	55.72	0.00	23.25	1.86	0.00	0.19	1.94	9.34	7.15	0.56	100.01	16.49	0.77
14	56.39	0.14	22.80	2.01	0.10	0.17	1.26	9.22	7.25	0.65	99.99	16.47	0.79
15	55.93	0.19	23.45	1.77	0.13	0.21	1.81	8.64	7.29	0.58	100.00	15.93	0.84
mean	**56.28**	**0.19**	**23.48**	**1.95**	**0.12**	**0.22**	**1.60**	**8.74**	**6.87**	**0.54**			
st dev	*1.04*	*0.08*	*0.50*	*0.29*	*0.08*	*0.07*	*0.19*	*0.58*	*0.62*	*0.09*			

L. Mezzano b

1	63.07	0.37	19.31	1.69	0.00	0.16	1.11	3.20	11.08	0.00	99.99	14.28	3.46
2	65.37	0.31	18.06	2.09	0.09	0.29	2.43	2.53	8.36	0.47	100.00	10.89	3.30
3	62.22	0.08	21.82	0.71	0.00	0.12	0.77	5.74	8.50	0.04	100.00	14.24	1.48
mean	**63.55**	**0.25**	**19.73**	**1.50**	**0.03**	**0.19**	**1.44**	**3.82**	**9.31**	**0.17**			
st dev	*1.63*	*0.15*	*1.91*	*0.71*	*0.05*	*0.09*	*0.88*	*1.69*	*1.53*	*0.26*			

P. di Pecore

	SiO_2	TiO_2	Al_2O_3	FeO_{tot}	MnO	MgO	CaO	Na_2O	K_2O	ClO	Total	Tot. alkali	K_2O/Na_2O
1	57.08	0.51	21.50	3.13	0.18	0.12	2.17	8.51	6.05	0.76	100.01	14.56	0.71
2	57.28	0.50	21.21	3.04	0.10	0.38	3.31	6.40	7.16	0.62	100.00	13.56	1.12
3	57.08	0.30	21.13	3.02	0.07	0.41	2.94	7.27	7.12	0.66	100.00	14.39	0.98
4	56.94	0.26	21.74	3.00	0.08	0.33	3.16	6.56	7.29	0.63	99.99	13.85	1.11
5	56.02	0.43	21.41	3.18	0.13	0.53	3.42	5.55	8.72	0.59	99.98	14.27	1.57
6	57.03	0.37	21.39	2.91	0.00	0.35	2.75	7.31	7.26	0.63	100.00	14.57	0.99
7	57.35	0.41	20.87	3.10	0.10	0.47	2.55	5.26	9.34	0.54	99.99	14.60	1.78
8	56.47	0.42	21.18	3.45	0.09	0.53	3.39	7.19	6.66	0.62	100.00	13.85	0.93
9	56.07	0.52	21.20	3.58	0.12	0.67	3.96	5.73	7.56	0.60	100.01	13.29	1.32
10	57.13	0.34	21.19	3.10	0.12	0.36	3.41	6.15	7.56	0.64	100.00	13.71	1.23
11	56.29	0.43	20.64	3.95	0.21	0.26	1.87	8.80	6.41	1.13	99.99	15.21	0.73
12	56.58	0.56	20.60	4.00	0.18	0.59	3.60	6.76	6.38	0.73	99.98	13.14	0.94
13	56.61	0.30	21.64	2.89	0.06	0.44	3.06	6.21	8.25	0.53	99.99	14.46	1.33
14	59.26	0.47	22.60	1.82	0.05	0.21	3.95	5.14	6.19	0.31	100.00	11.33	1.20
15	56.16	0.14	21.63	3.07	0.14	0.50	3.12	6.01	8.57	0.67	100.00	14.58	1.43
16	56.96	0.14	21.87	3.08	0.14	0.49	3.06	5.96	7.66	0.65	100.00	13.62	1.29
mean	**56.89**	**0.38**	**21.36**	**3.14**	**0.11**	**0.42**	**3.11**	**6.55**	**7.39**	**0.64**			
st dev	*0.77*	*0.13*	*0.49*	*0.49*	*0.05*	*0.14*	*0.57*	*1.06*	*0.96*	*0.16*			

Basento basin

	SiO_2	TiO_2	Al_2O_3	FeO_{tot}	MnO	MgO	CaO	Na_2O	K_2O	ClO	Total	Tot. alkali	K_2O/Na_2O
1	55.38	0.49	20.83	4.08	0.00	0.84	4.41	4.80	8.60	0.57	100.00	13.40	1.79
2	55.17	0.58	20.90	4.27	0.00	0.97	4.28	4.77	8.45	0.60	99.99	13.22	1.77
3	56.67	0.41	20.97	3.37	0.00	0.52	3.21	4.93	9.41	0.51	100.00	14.34	1.91
4	55.72	0.41	20.72	4.19	0.00	0.85	4.32	4.57	8.65	0.58	100.01	13.22	1.89
5	55.99	0.43	20.75	3.91	0.00	0.74	3.92	4.95	8.81	0.50	100.00	13.76	1.78

6	56.29	0.44	23.38	2.24	0.00	0.31	6.24	4.67	6.12	0.31	100.00	10.79	1.31
7	54.95	0.57	20.79	3.99	0.00	0.81	3.77	6.09	8.45	0.60	100.02	14.54	1.39
8	55.17	0.69	20.50	4.54	0.00	0.90	4.91	4.61	8.11	0.57	100.00	12.72	1.76
9	55.84	0.70	20.52	4.45	0.00	0.69	3.82	6.23	7.08	0.67	100.00	13.31	1.14
10	55.69	0.49	20.97	4.00	0.00	0.77	4.17	5.05	8.30	0.55	99.99	13.35	1.64
11	55.22	0.33	21.01	4.01	0.00	0.85	4.18	5.38	8.40	0.61	99.99	13.78	1.56
12	56.68	0.56	21.17	3.23	0.00	0.56	4.09	4.71	8.48	0.52	100.00	13.19	1.80
13	55.69	0.53	20.94	4.01	0.00	0.73	4.18	4.68	8.65	0.59	100.00	13.33	1.85
mean	**55.73**	**0.51**	**21.03**	**3.87**	**0.00**	**0.73**	**4.27**	**5.03**	**8.27**	**0.55**			
st dev	*0.56*	*0.11*	*0.73*	*0.61*	*0.00*	*0.18*	*0.71*	*0.55*	*0.83*	*0.09*			

	RF93-30		**IN68-9**		**LGM**		**LNEMI**		**ACC**	**EU2**		**EU3**		**EU5**a		**EU5**b	
	530 cm	*sd*	20 cm	*sd*	TM-4	*sd*	450 cm	*sd*	563 cm		*sd*		*sd*		*sd*		*sd*
SiO_2	55.93	*0.57*	55.79	*0.36*	55.91	*0.95*	55.82	*1.00*	56.08	56.89	*1.60*	55.63	*0.60*	57.53	*1.15*	65.71	*2.20*
TiO_2	0.36	*0.08*	0.17	*0.05*	0.13	*0.02*	0.02	*0.03*	0.18	0.08	*0.11*	0.31	*0.10*	0.35	*0.22*	0.42	*0.39*
Al_2O_3	20.61	*0.50*	21.62	*0.35*	23.44	*0.31*	23.12	*0.33*	23.47	23.89	*0.64*	21.85	*0.50*	21.76	*1.50*	18.19	*0.82*
FeO_{tot}	4.07	*0.25*	3.09	*0.27*	1.43	*0.24*	1.63	*0.28*	1.41	1.52	*0.38*	3.07	*0.46*	3.11	*1.05*	2.26	*0.66*
MnO	0.07	*0.06*	0.11	*0.04*	0.11	*0.02*	0.07	*0.05*	0.12	0.12	*0.10*	0.00	*0.00*	0.13	*0.12*	0.19	*0.14*
MgO	0.6	*0.10*	0.45	*0.20*	0.06	*0.02*	0.1	*0.05*	0.08	0.00	*0.00*	0.09	*0.08*	0.57	*0.46*	0.34	*0.15*
CaO	4.43	*0.83*	3.80	*0.40*	1.64	*0.24*	1.96	*0.74*	1.77	1.61	*0.32*	4.46	*0.92*	3.41	*1.11*	2.31	*0.42*
Na_2O	4.91	*0.36*	6.35	*0.38*	8.83	*0.43*	9.46	*1.17*	9.17	6.50	*2.39*	5.57	*0.52*	5.14	*1.30*	2.81	*0.55*
K_2O	8.47	*0.92*	8.12	*0.15*	7.82	*0.48*	7.26	*1.01*	7.72	8.41	*1.37*	8.23	*0.49*	7.39	*0.53*	7.24	*1.02*
ClO	0.55	*0.06*	0.50	*0.05*	0.4	*0.23*	0.56	*0.05*	-	0.83	*0.18*	0.63	*0.13*	0.60	*0.11*	0.53	*0.23*
Total	100.00	-	100.00	-	99.77	-	100.00	-	100.00	99.86	-	99.84	-	100.00	-	100.00	-
Tot. alkali	13.38	-	14.47	-	16.65	-	16.72	-	16.89	14.92	-	13.80	-	12.53	-	10.05	-
K_2O/Na_2O	1.73	-	1.28	-	0.89	-	0.77	-	0.84	1.29	-	1.48	-	1.44	-	2.57	-

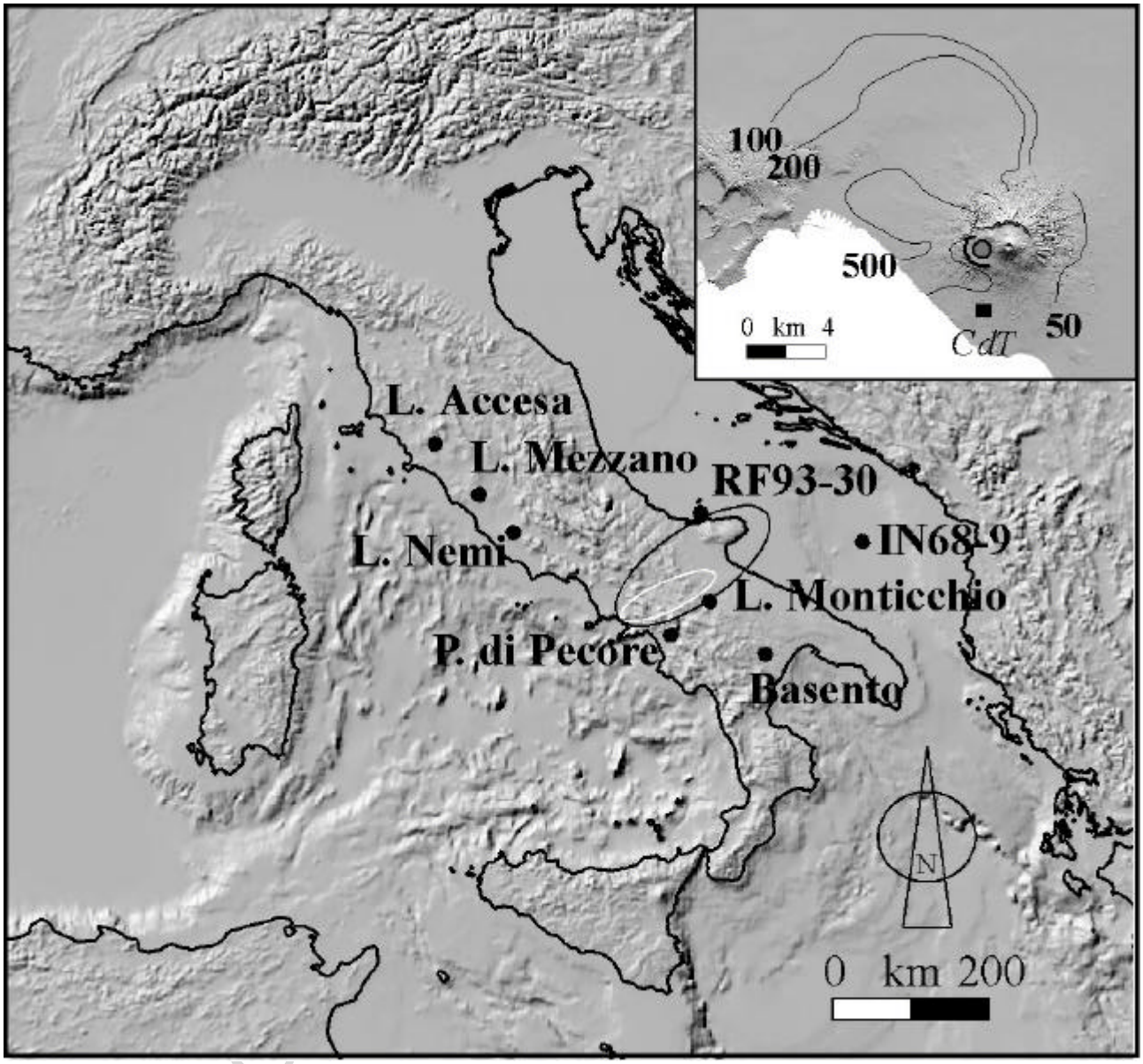

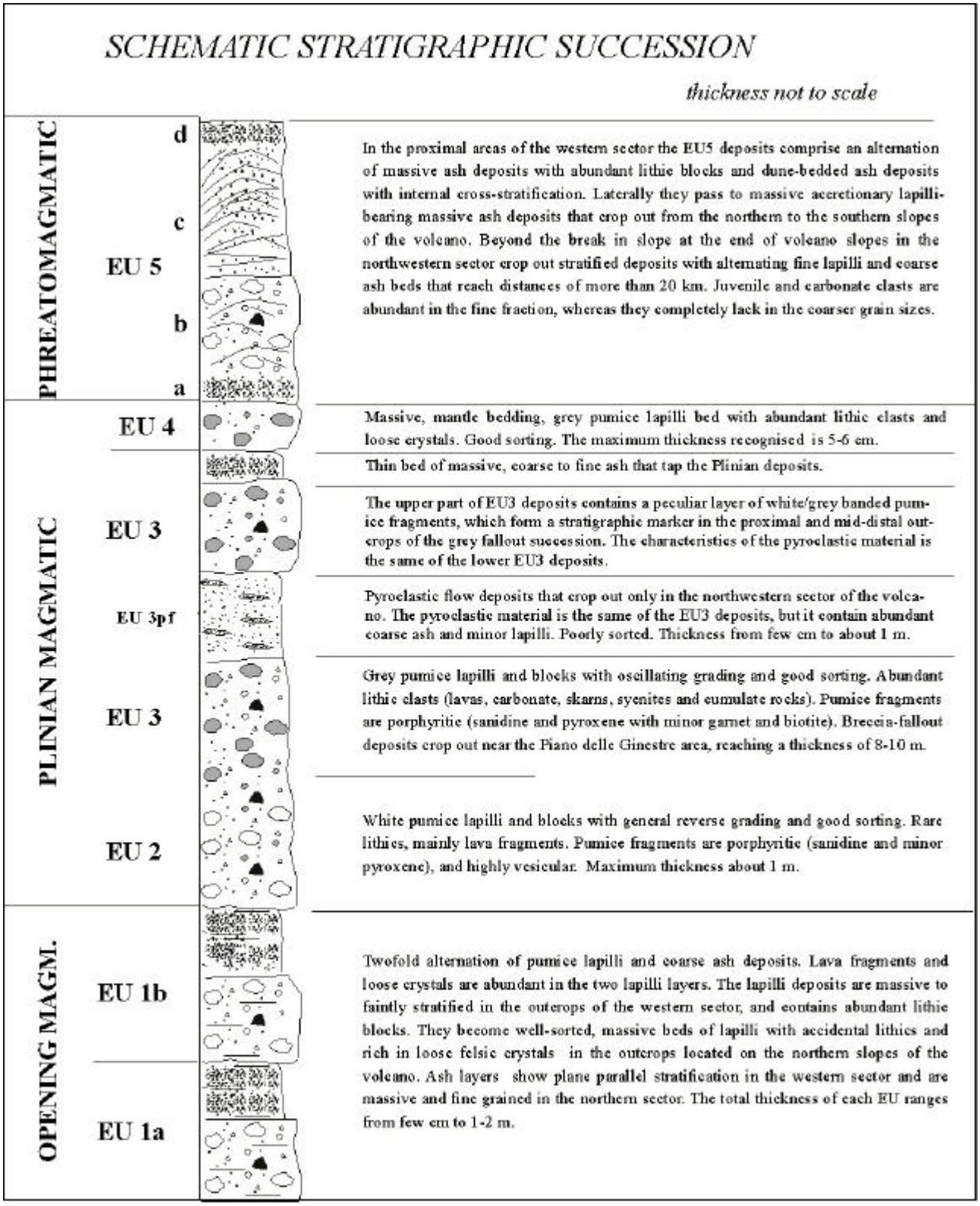

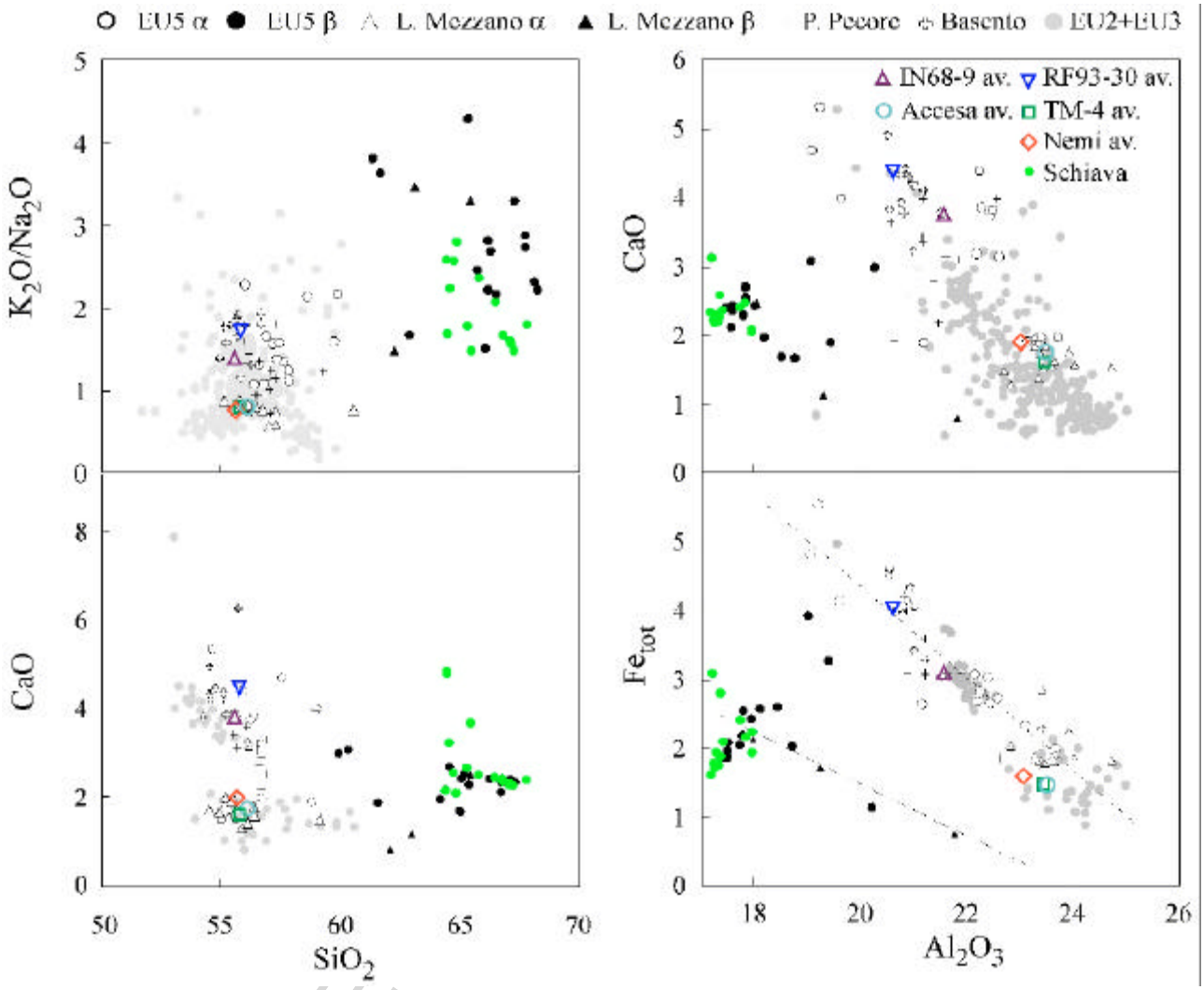

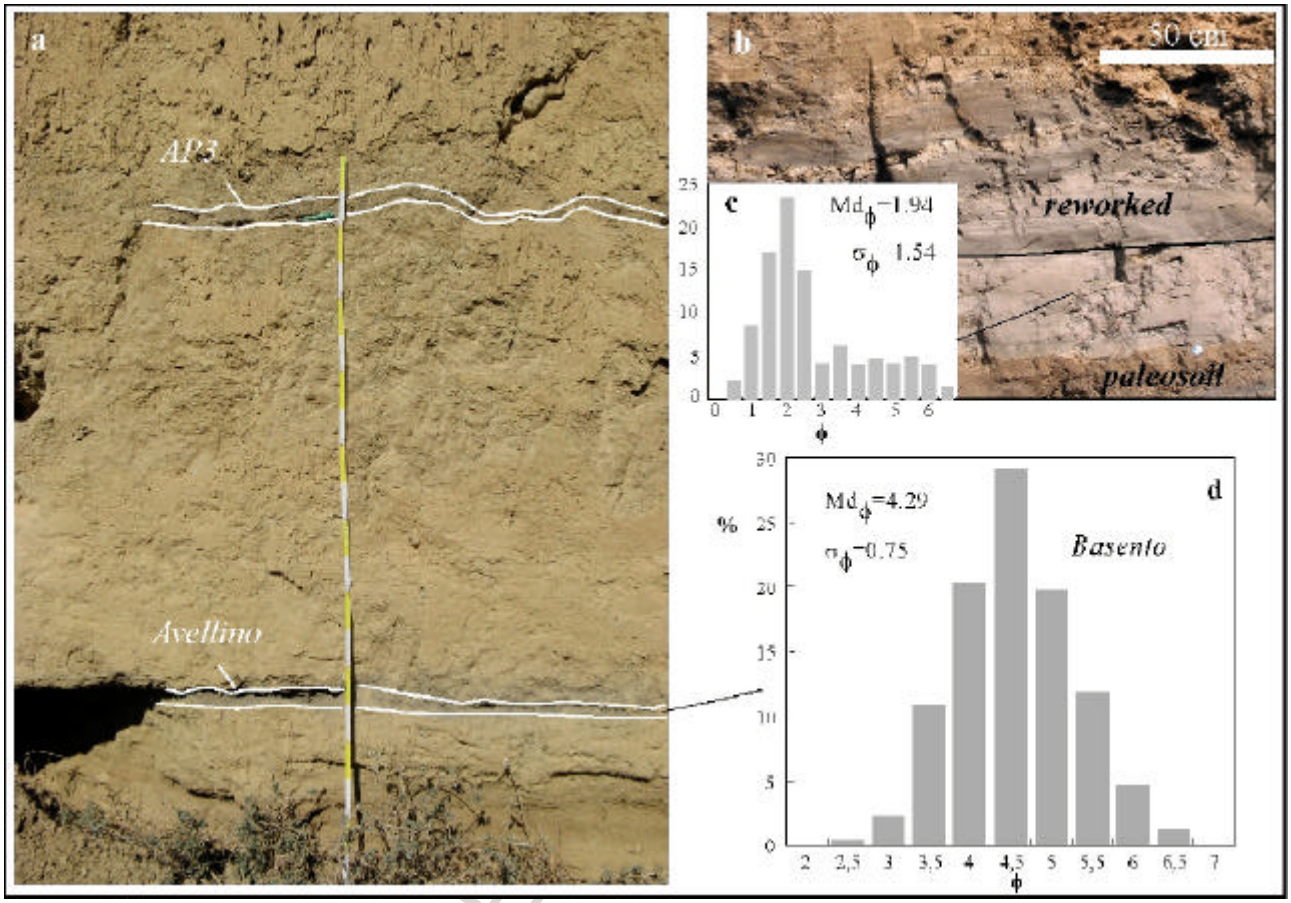

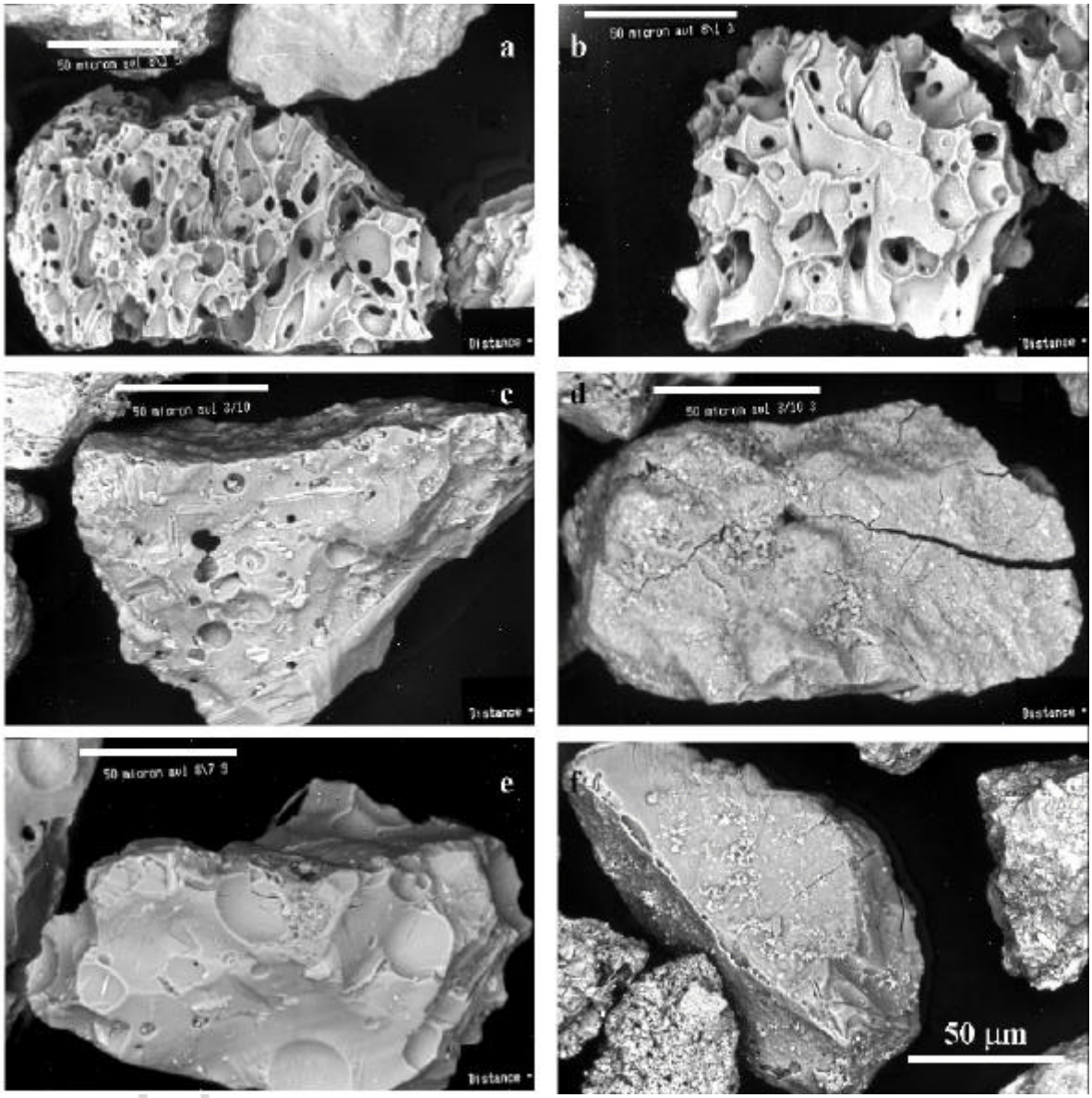

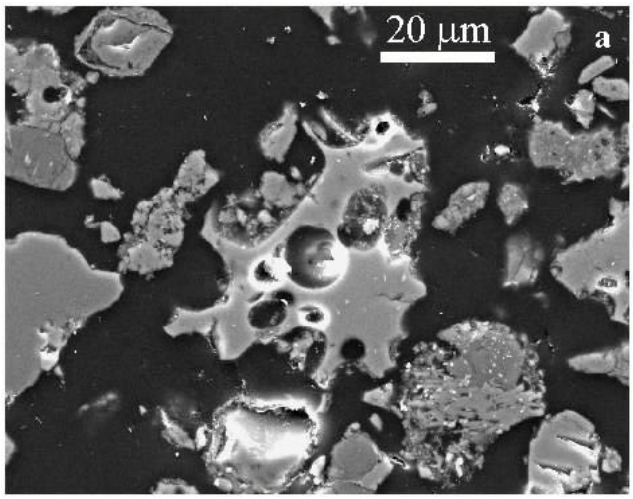

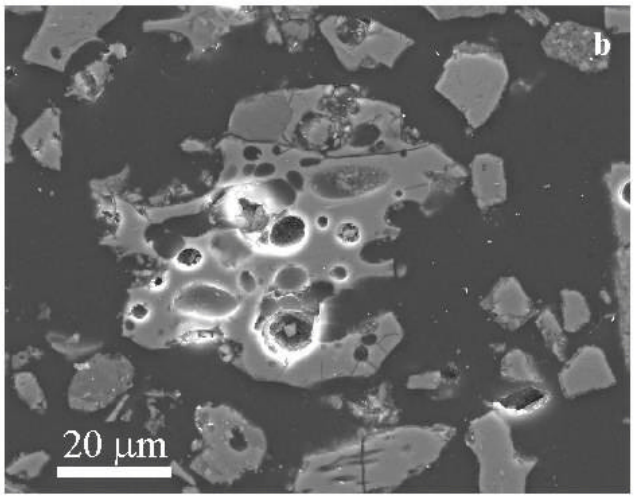

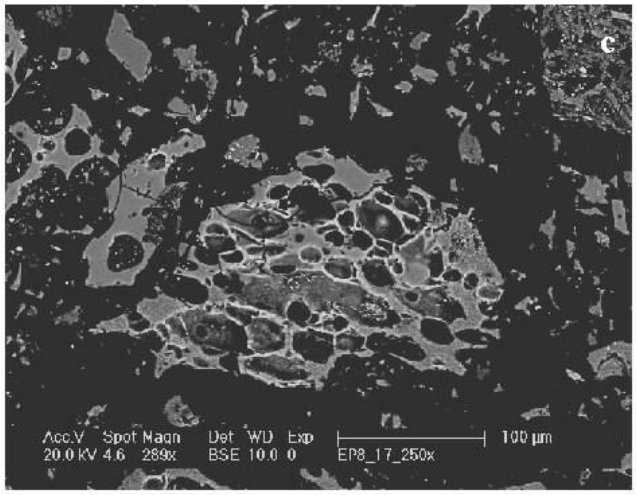

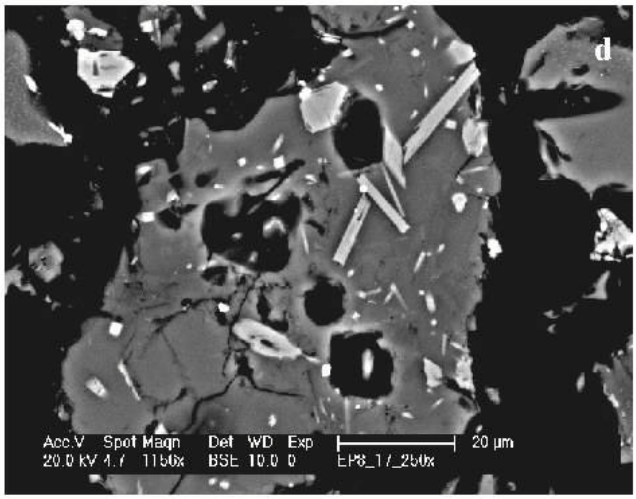

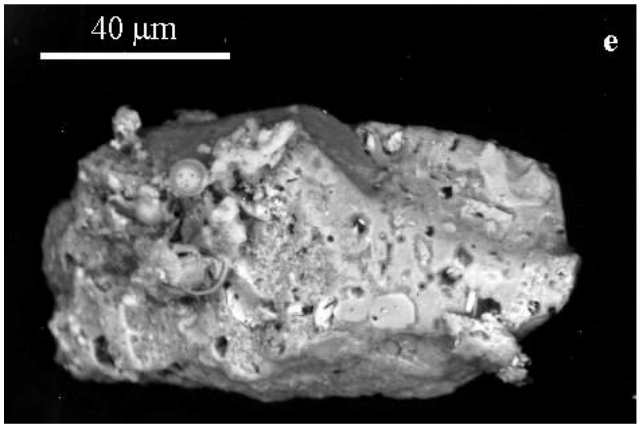

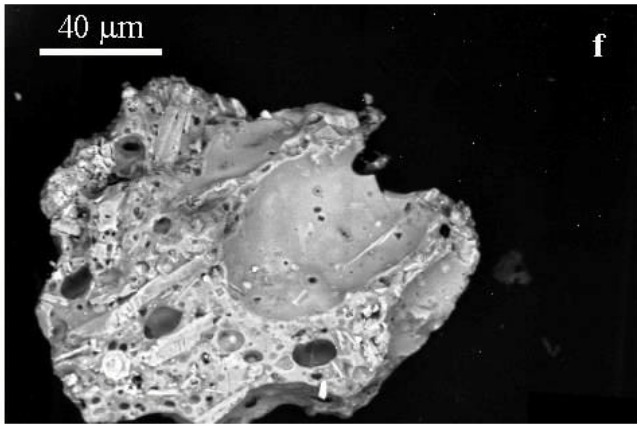

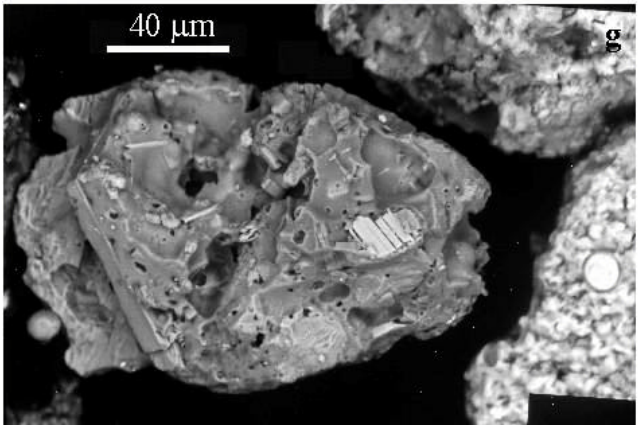

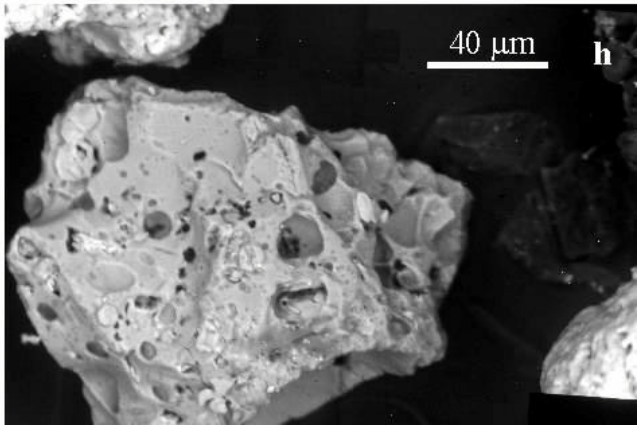

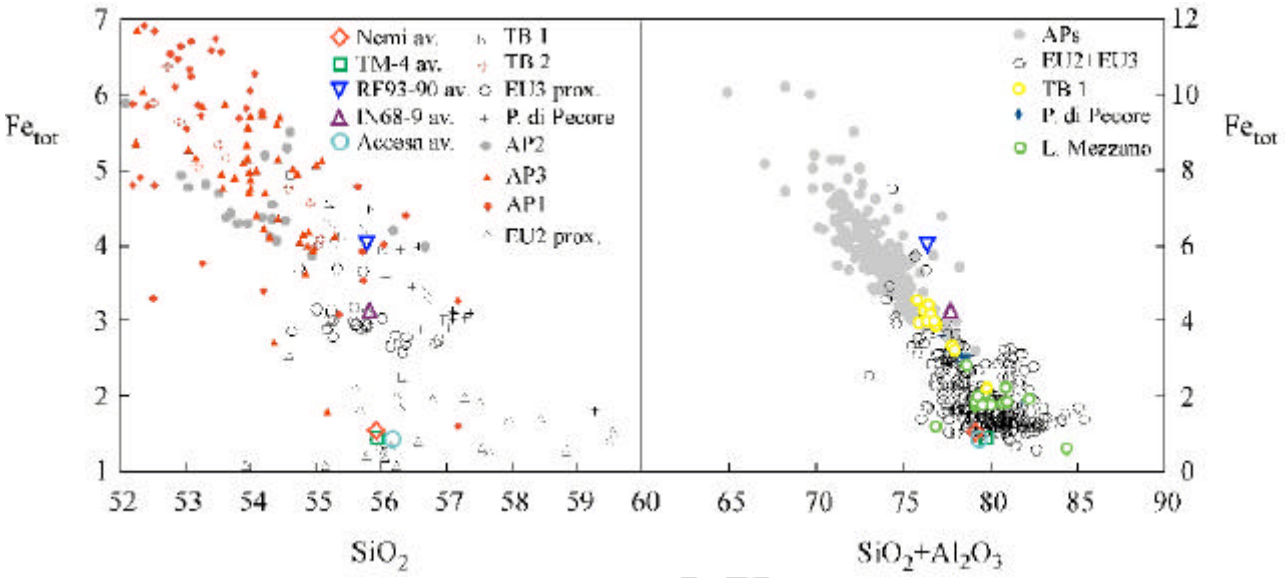

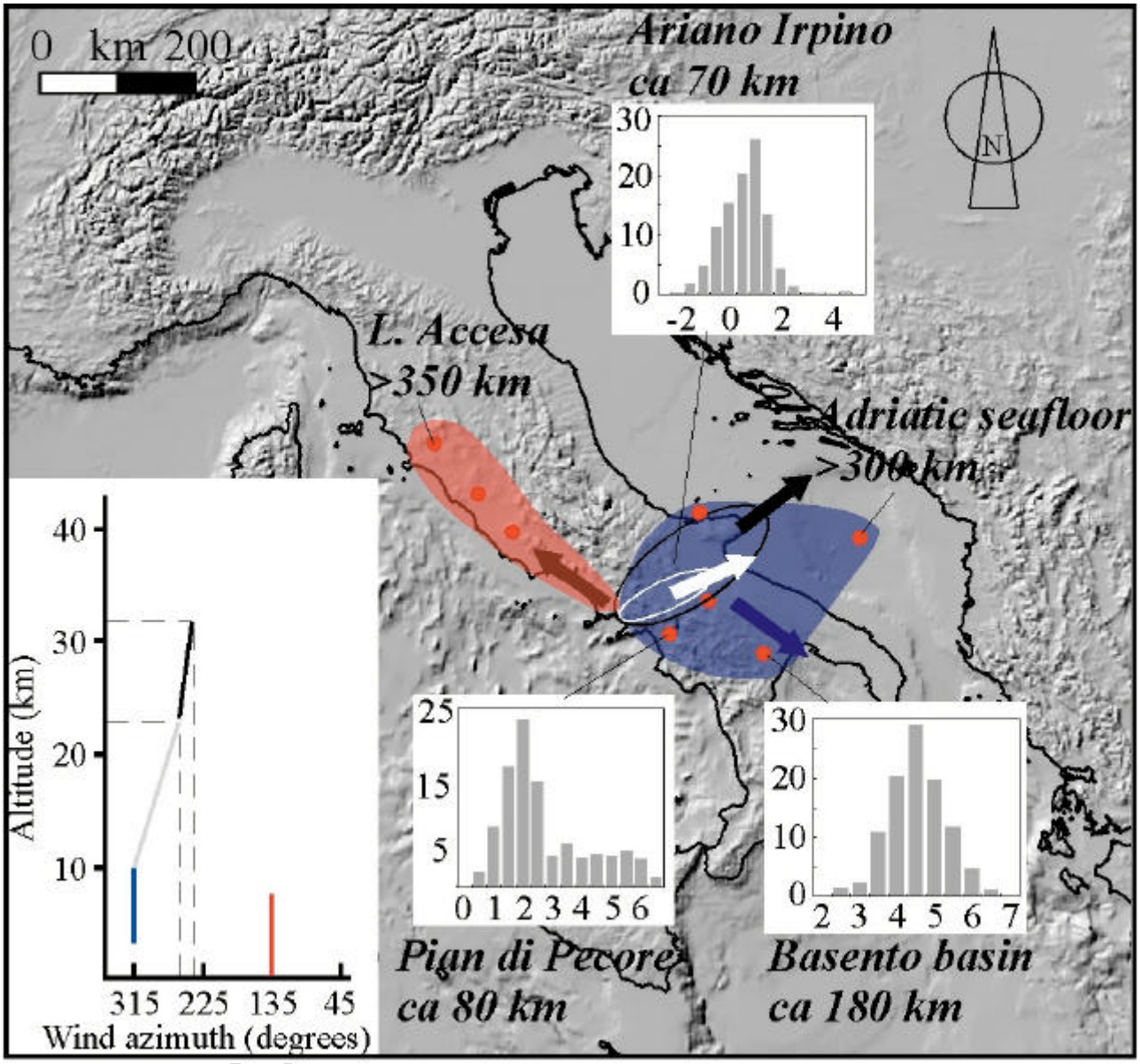
0 km 200
Ariano Irpino
ca 70 km
N
L. Accesa
>350 km
Adriatic seafloor
>300 km
Altitude (km)
Wind azimuth (degrees)
Pian di Pecore
ca 80 km
Basento basin
ca 180 km